














ARTICLE

iNKT cell-neutrophil crosstalk promotes colorectal cancer pathogenesis

Georgia Lattanzi ^{1,2,†}, Francesco Strati ^{1,3,†}, Angélica Díaz-Basabe^{1,2}, Federica Perillo ^{1,2}, Chiara Amoroso⁴, Giulia Protti ³, Maria Rita Giuffrè¹, Luca Iachini ³, Alberto Baeri ³, Ludovica Baldari⁵, Elisa Cassinotti ⁵, Michele Ghidini⁶, Barbara Galassi⁶, Gianluca Lopez ⁷, Daniele Noviello ^{4,8}, Laura Porretti⁹, Elena Trombetta ⁹, Eleonora Messuti ¹, Luca Mazzarella¹, Giandomenica Iezzi ¹⁰, Francesco Nicassio¹¹, Francesca Granucci³, Maurizio Vecchi^{4,8}, Flavio Caprioli^{4,8} and Federica Facciotti ^{1,3,✉}

© 2023 The Author(s). Published by Elsevier Inc. on behalf of Society for Mucosal Immunology.
This is an open access article under the CC BY license (<http://creativecommons.org/licenses/by/4.0/>).

iNKT cells account for a relevant fraction of effector T-cells in the intestine and are considered an attractive platform for cancer immunotherapy. Although iNKT cells are cytotoxic lymphocytes, their functional role in colorectal cancer (CRC) is still controversial, limiting their therapeutic use. Thus, we examined the immune cell composition and iNKT cell phenotype of CRC lesions in patients (n = 118) and different murine models. High-dimensional single-cell flow-cytometry, metagenomics, and RNA sequencing experiments revealed that iNKT cells are enriched in tumor lesions. The tumor-associated pathobiont *Fusobacterium nucleatum* induces IL-17 and Granulocyte-macrophage colony-stimulating factor (GM-CSF) expression in iNKT cells without affecting their cytotoxic capability but promoting iNKT-mediated recruitment of neutrophils with polymorphonuclear myeloid-derived suppressor cells-like phenotype and functions. The lack of iNKT cells reduced the tumor burden and recruitment of immune suppressive neutrophils. iNKT cells *in-vivo* activation with α -galactosylceramide restored their anti-tumor function, suggesting that iNKT cells can be modulated to overcome CRC-associated immune evasion. Tumor co-infiltration by iNKT cells and neutrophils correlates with negative clinical outcomes, highlighting the importance of iNKT cells in the pathophysiology of CRC. Our results reveal a functional plasticity of iNKT cells in CRC, suggesting a pivotal role of iNKT cells in shaping the tumor microenvironment, with relevant implications for treatment.

Mucosal Immunology (2023) 16:326–340; <https://doi.org/10.1016/j.mucimm.2023.03.006>

INTRODUCTION

Invariant natural killer T cells (iNKT) are a lipid-specific, evolutionary-conserved population of lymphocyte positioned at the interface between innate and adaptive immunity¹. Microbial and endogenous^{2,3} signals finely tune iNKT cell functions, including tissue immune surveillance⁴ and first-line defense against infectious microorganisms¹. iNKT cells are present in the intestinal lamina propria as tissue-resident cells, and variations in the gut microbiota composition can rapidly alter their phenotype^{1,5}. Dysbiosis imprints iNKT cells toward a pro-inflammatory phenotype⁶, whereas normobiosis restoration upon fecal microbiota transplantation and exposure to short-chain fatty acids induce their production of regulatory cytokines, such as interleukin (IL) 10^{7,8}. Along with the patrolling of tissue integrity, iNKT cells actively participate in the immune surveillance against malignant transformation and tumor progression, including human colorectal cancer (CRC)⁹. CRC is the 3rd most

prevalent cancer worldwide and the 2nd leading cause of cancer-related death¹⁰. Microbiota-elicited inflammation is an important contributor to CRC pathogenesis, regardless of pre-cancer inflammatory history¹¹. Because of their fast responsiveness to microbes, iNKT cells can produce a large amount of effector cytokines¹ during the time required for the recruitment, activation, and expansion of conventional T cells¹², with the potential to robustly imprint the tumor microenvironment (TME) and the CRC developmental trajectory. iNKT cells are considered important in anti-tumor immunity⁹, and their infiltration in tumor lesions is a positive prognostic factor in different cancer types^{13,14}. Moreover, iNKT cells possess cytotoxic properties and are endowed with cell-killing activities toward different human CRC cell lines and the primary patient's derived cancer epithelial cells through the perforin-granzyme pathway¹⁵. However, their role in CRC progression has never been fully elucidated and it is still controversial^{13,16}. Indeed, iNKT cells with a pro-

¹Department of Experimental Oncology, European Institute of Oncology IRCCS, Milan, Italy. ²Department of Oncology and Hemato-oncology, Università degli Studi di Milano, Milan, Italy. ³Department of Biotechnology and Biosciences, University of Milano-Bicocca, Milan, Italy. ⁴Gastroenterology and Endoscopy Unit, Fondazione IRCCS Cà Granda, Ospedale Maggiore Policlinico, Milan, Italy. ⁵General and Emergency Surgery Unit, Fondazione IRCCS Cà Granda, Ospedale Maggiore Policlinico, Milan, Italy. ⁶Medical Oncology, Fondazione IRCCS Cà Granda, Ospedale Maggiore Policlinico, Milan, Italy. ⁷Pathology Unit, Fondazione IRCCS Cà Granda, Ospedale Maggiore Policlinico, Milan, Italy. ⁸Department of Pathophysiology and Transplantation, Università degli Studi di Milano, Milan, Italy. ⁹Clinical Chemistry and Microbiology Laboratory, Fondazione IRCCS Cà Granda Ospedale Maggiore Policlinico, Milan, Italy. ¹⁰Department of Visceral Surgery, EOC Translational Research Laboratory, Bellinzona, Switzerland. ¹¹Center for Genomic Science of IIT@SEMM, Istituto Italiano di Tecnologia (IIT), Milan, Italy. [✉] email: federica.facciotti@unimib.it

tumorigenic phenotype have been described in murine models of CRC and associated with shorter disease-free survival in patients^{16,17}. Here, by taking advantage of a large cohort of patients with human CRC and of different murine models of colon carcinogenesis, we address the contribution of iNKT cells to CRC pathophysiology and the effect of the tumor-associated microbiota in shaping their functions. We demonstrate that tumor-infiltrating iNKT cells, but not those isolated from adjacent tumor-free areas, manifest a pro-tumorigenic phenotype and correlate with negative disease outcomes in patients with CRC. We show that the CRC-associated pathobiont *Fusobacterium nucleatum* (*Fn*) promotes iNKT cell-mediated recruitment of neutrophils with a polymorphonuclear myeloid-derived suppressor cells (PMN-MDSCs) phenotype. Finally, we show that restoring the cytotoxic potential of iNKT cells by *in vivo* treatment with the iNKT-specific agonist α -galactosylceramide (α GalCer) leads to the control of tumor growth.

RESULTS

Tumor-infiltrating human iNKT cells show a pro-tumorigenic profile and correlate with tumor-associated neutrophils (TANs) infiltration

To uncover the role of iNKT cells in human CRC, we collected freshly isolated surgical specimens from 118 patients with CRC enrolled at the Policlinico Hospital Milan, whose clinical features are described in Table 1.

The immunophenotyping by manual gating analysis of multiparameter flow cytometry of tumor lesions (TUMs), as well as adjacent non-tumor colon tissue (NCT), revealed that iNKT cells are significantly enriched in TUM samples (Fig. 1A, Supplementary Fig. 1A). By applying a phenograph unsupervised clustering (Supplementary Figs. 2A and 2B), we identified a cluster of iNKT cells (cluster C16) specifically enriched in TUM (Fig. 1B, Supplementary Figs. 2A and 2B); the metaclustering analysis of cluster C16 revealed that tumor-infiltrating iNKT cells are characterized by an overall increased expression of IL17 and GM-CSF (clusters C1 and C2), whereas interferon (IFN) γ is expressed mainly by NCT-infiltrating iNKT cells (cluster C4, Fig. 1C). The manual gating analysis confirmed the increased frequency of GM-CSF⁺IL17⁺iNKT cells in CRC lesions and of IFN γ ⁺iNKT cells in NCT (Figs. 1D and 1E). The

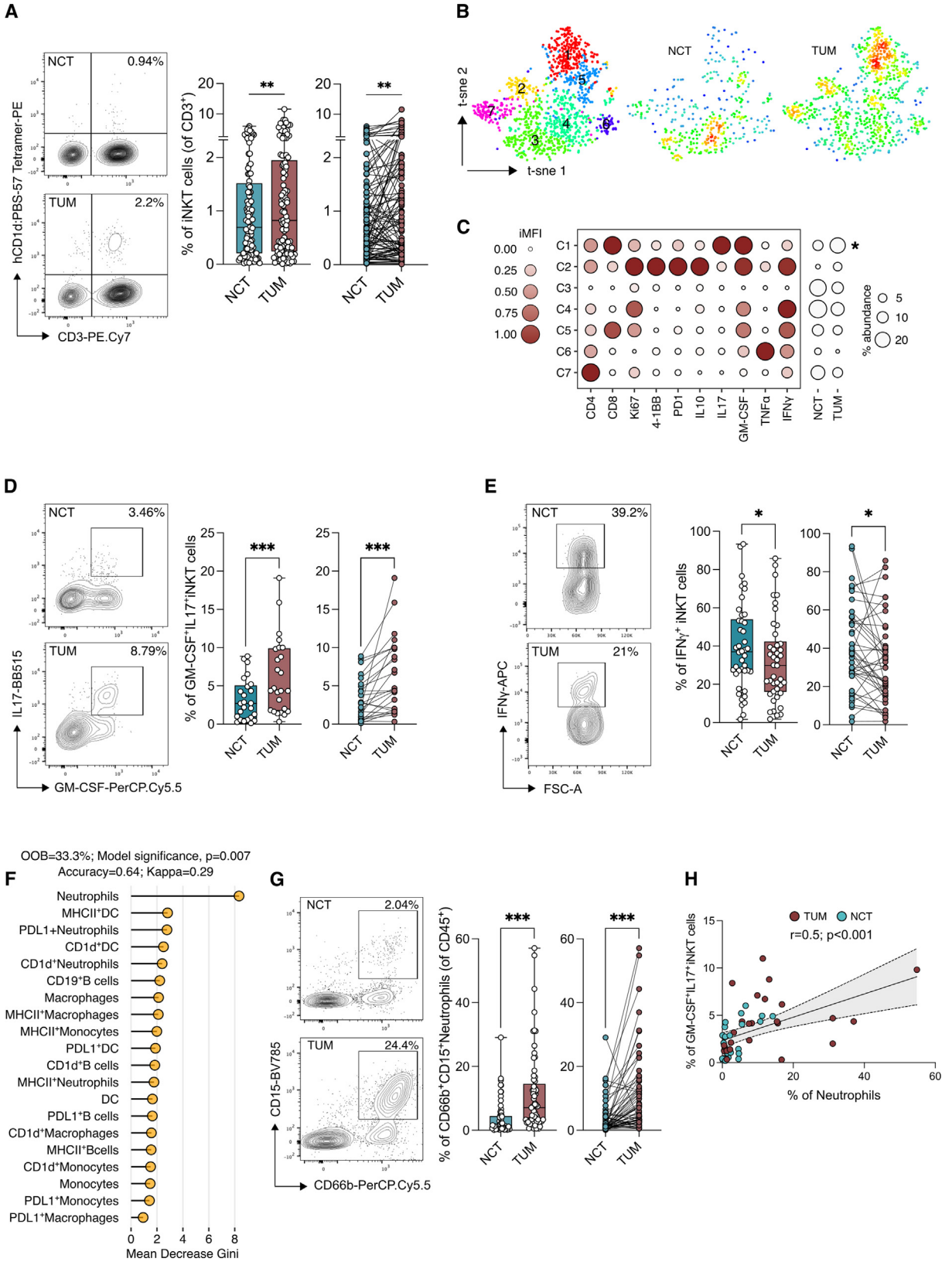
co-expression of IL17 and GM-CSF was a unique feature of iNKT cells, distinguishing them from other tumor-infiltrating conventional (clusters of differentiation [CD4]⁺ and CD8⁺) and unconventional ($\gamma\delta$ T and Mucosal-associated invariant T cells (MAIT)) T cells (Supplementary Figs. 2C and 2D). Phenotypically, the manual gating analysis of Fluorescence Activated Cell Sorting (FACS) data showed an increased expression of exhaustion/inhibitory molecules, including PD-1, TIGIT, and TIM-3 (Supplementary Fig. 2E) and a reduced expression of activation markers, such as CD69, CD161, and CD137 (4-1BB) in tumor-infiltrating iNKT cells compared with NCT (Supplementary Fig. 2F). No differences were observed for the secretion of other cytokines and cytotoxic molecules compared with NCT; although, we observed a decreased expression of the pro-apoptotic factor Fas ligand in tumor-infiltrating iNKT cells (Supplementary Figs. 2G and 2H). These data collectively indicate that tumor-infiltrating iNKT cells are skewed toward a pro-tumorigenic phenotype, characterized by the secretion of GM-CSF, IL17, and the expression of exhaustion/inhibitory molecules.

iNKT cells can modulate the activity of myeloid cells during homeostasis, inflammation and tumor development¹⁸. Thus, we hypothesized that tumor-infiltrating iNKT cells may shape the TME by acting primarily on innate immune cells. A random forest-based classification modeling identified neutrophils (CD45⁺CD66b⁺CD15⁺ cells, Supplementary Fig. 1B) as the most important innate immune cell population (Supplementary Fig. 3A) to classify samples according to their location (i.e. TUM vs. NCT) (Fig. 1F). Neutrophils were significantly enriched in CRC lesions (Fig. 1G), had a mature (CD33^{mid}CD10⁺CD16⁺), aged-like phenotype (CD62L⁻CXCR4⁺), and downregulated the expression of the antigen-presenting molecules CD1d and Major histocompatibility complex (MHC)-II (MHC-II) (Supplementary Figs. 3B and 3C). No differences were detected in the expression of the immune checkpoint programmed death-ligand 1 (PD-L1, Supplementary Fig. 3C). Most importantly, neutrophils correlated with the frequency of GM-CSF⁺IL17⁺iNKT cells (Spearman's $r = 0.5$, $p < 0.001$, Fig. 1H) but not with total iNKT cells (Supplementary Fig. 3D), suggesting a specific crosstalk between T helper 17-like iNKT cells and TANs. Altogether, these data suggest the existence of a functional iNKT-TAN axis in CRC.

Table 1. Clinical characteristics of the study population.

	All patients [n = 118]	Stage 0/I [n = 4/25]	Stage II [n = 38]	Stage III [n = 51]
Male/Female, n.	64/54	14/15	24/14	25/26
Age at enrollment, mean \pm SD	70 [\pm 12.5]	71.7 [\pm 12.5]	71.8 [\pm 10.9]	67.7 [\pm 14.1]
Male	69 [\pm 12.7]	72.6 [\pm 10.4]	71.3 [\pm 11]	68.5 [\pm 14.2]
Female	69.5 [\pm 13]	71.2 [\pm 13.8]	72.75 [\pm 10.2]	66.8 [\pm 14.3]
Disease Location				
Left-side colon (CSX)	66	20	18	28
Right-side colon (CDX)	52	9	20	23
MMR status				
Proficient/Deficient	103/15	27/2	32/6	44/7
Therapy				
Neoadjuvant CT-RT	9	5	1	3
Adjuvant CT	21	1	6	14
CAPOX	13	1	1	11
Capecitabine	6	-	5	1
Relapse	8	1	-	7

CAPOX = capecitabine and oxaliplatin; CT = chemotherapy; CT-RT = chemotherapy-radiotherapy.



Tumor-associated *Fn* induces a pro-tumorigenic signature in iNKT cells and favors neutrophil recruitment

The gut microbiota is an oncogenic driver of CRC¹⁹ and intestinal microbes represent potent stimulators of iNKT cell responses⁶. Thus, we analyzed the tumor-associated microbiota from a sub-study cohort of our patients (Supplementary Table 1) by 16S rRNA gene sequencing and identified *Fusobacterium* as one of the most enriched amplicon sequence variant in TUM versus NCT (Fig. 2A). *Fn* is a hallmark of CRC, extensively studied for its pro-tumorigenic properties¹⁹, but its effect on iNKT cells has never been tested. Thus, we primed the intestinal and circulating human iNKT cell lines^{6,15} with monocyte-derived dendritic cells (moDCs) pulsed with *Fn* or α GalCer, the prototype agonist of iNKT cells²⁰, and performed *in vitro* functional and cytotoxic assays, as well as RNA sequencing of iNKT cells (Fig. 2B). The exposure of iNKT cells to *Fn* did not affect the *in vitro* cytotoxic functions against colon adenocarcinoma cell lines (Fig. 2C). However, *Fn*-primed iNKT cells showed an enriched neutrophil chemotaxis gene signature, which included the chemokines of the C-X-C and C-C motif ligand family genes *CXCL8*, *CXCL2*, *CXCL3*, *CCL3L1*, *CCL4L2*, *CCL20*, and *CCL22* (Figs. 2D and 2E). By contrast, α GalCer-primed iNKT cells presented an IFN γ /cytotoxic-related gene signature, including the expression of *TBX21*, *IFNG*, *PFN1*, *GPLY*, *GZMA*, *GZMB*, *GZMH*, *LTA*, *LTB*, and *NKG7* (Fig. 2D). Consistently, α GalCer-primed iNKT cells secreted IFN γ , whereas *Fn* induced the production of GM-CSF and IL17 (Fig. 2F). *Fn*-primed iNKT cells upregulated the expression of neutrophil chemotaxis genes, such as *CXCL8*, *CCL3L1*, *CCL4L2*, and *CCL20*, also compared with the non-stimulated control, the latter still expressing the cytotoxic-related genes *GZMA*, *PFN1*, and *GPLY* (Supplementary Fig. 4). Because iNKT cells may impact on neutrophil survival, recruitment, and activation status^{21–23}, we evaluated how *Fn* affected the crosstalk between iNKT cells and neutrophils. Both *Fn*- and α GalCer-primed iNKT cells increased the survival rate of neutrophils compared with unstimulated cells (Supplementary Figs. 5A and 5B). However, only *Fn*-primed iNKT cells induced neutrophil recruitment (Fig. 2G), in line with the upregulation of *CXCL8* (Fig. 2D) and the higher concentration of IL8 in the iNKT cell-derived culture supernatant (Fig. 2H). Neutrophil migration was inhibited by the use of reparixin, i.e. an allosteric inhibitor of the IL8 receptor (CXCR-1/-2), demonstrating that neutrophil chemotaxis is induced by chemokines produced by *Fn*-primed iNKT cells (Fig. 2G). Moreover, *Fn*-primed iNKT cells affected neutrophil activation status by reducing their respiratory burst capability, inducing the expression of PD-L1 (Supplementary Figs. 5C and 5D) and promoting their suppressive activity toward CD4⁺T cell proliferation (Fig. 2I). These results suggest that iNKT cells functional shaping by CRC-associated microbiota promotes neutrophils recruitment and their immunosuppressive phenotype.

Absence of iNKT cells limits tumor burden by reducing pro-tumorigenic TANs

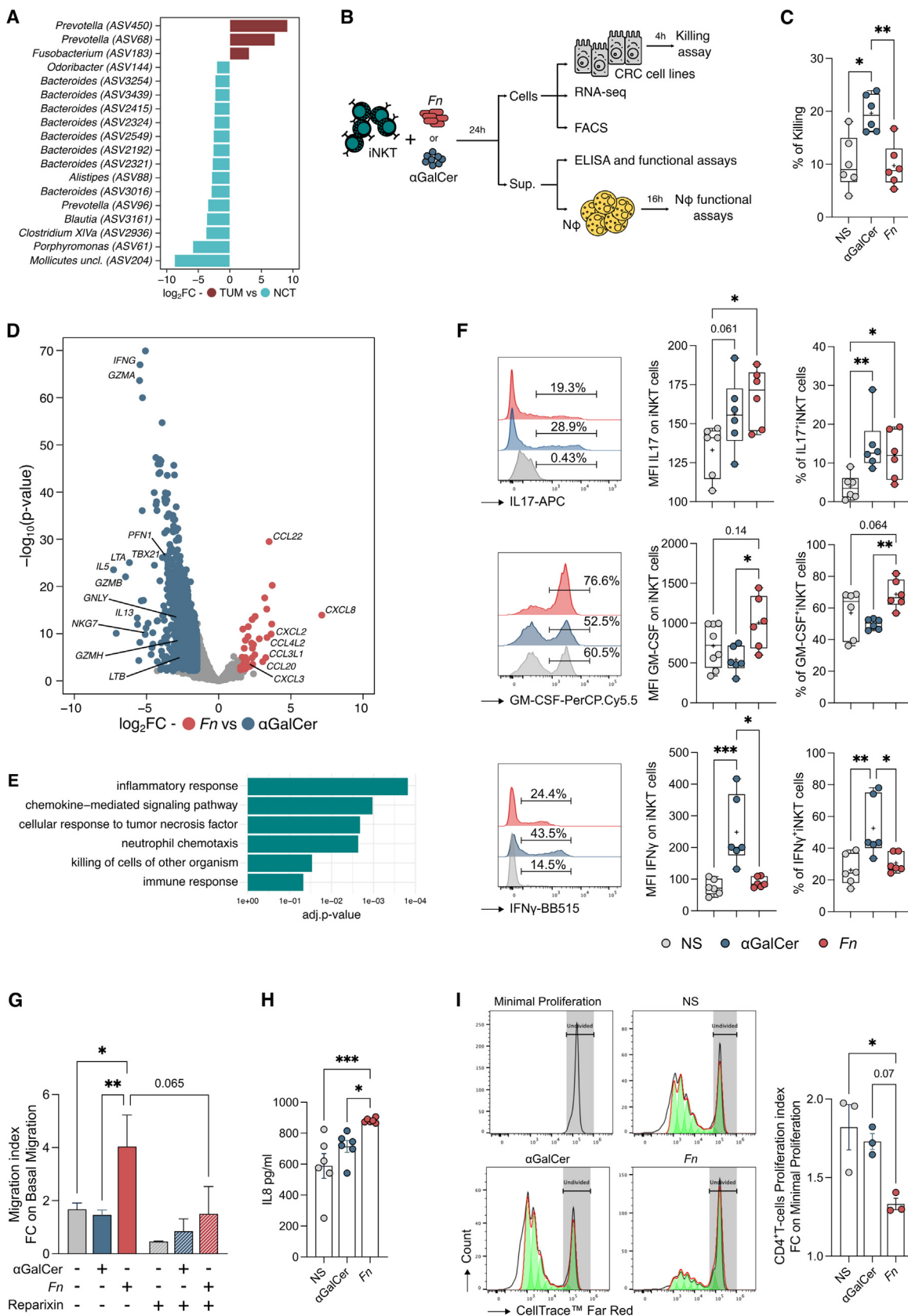
To functionally dissect the dynamic interaction between iNKT cells and neutrophils in CRC, we induced colorectal tumorigenesis using the chemical azoxymethane-dextran sodium sulfate (AOM-DSS) model of colitis-associated CRC.

Because mucosal iNKT cells are largely tissue-resident lymphocytes¹², they might infiltrate tumors at the initial steps of their formation and affect the TME by modulating neutrophil behavior. To test this hypothesis, we first evaluated the dynamics of tumor growth and intratumor frequency of iNKT cells and neutrophils in the AOM-DSS model (Supplementary Figs. 6A and 6B). Tumor-infiltrating iNKT cells reached their peak abundance between day 21 and day 28 from tumor induction (Supplementary Fig. 6A). Conversely, the kinetic of neutrophils infiltration started at day 35 and increased until day 42; then, both neutrophils and iNKT cells abundance declined (Supplementary Fig. 6A). At this time point, i.e. day 49 from tumor induction (T1), the AOM-DSS model mirrored the key phenotypic and functional features of tumor-infiltrating iNKT cells (Supplementary Figs. 6C and 6D) and neutrophils (Supplementary Figs. 5E and 5F) observed in our human cohort. Interestingly, at later time points from tumor induction, i.e. day 70 (T2), tumor-infiltrating iNKT cells began to lose the key features observed in patients with CRC (Supplementary Figs. 6G and 6H), prompting us to focus on the early time point (T1) *in vivo*.

To rule out the anti- or pro-tumorigenic role of iNKT cells in CRC, we induced tumorigenesis in animals lacking iNKT cells, i.e. *CD1d*^{-/-} and *Traj18*^{-/-} mice. Both iNKT cell-deficient strains showed a reduced tumor formation compared with wild-type C57BL/6 (B6) mice (Figs. 3A–C).

The abundance of TANs was significantly reduced in *CD1d*^{-/-} and *Traj18*^{-/-} compared with iNKT cell-proficient mice (Fig. 3D). Moreover, *Traj18*^{-/-} TANs negatively correlated with the number of tumors, whereas the tumors increased proportionally with TANs in B6 mice (Fig. 3E). Next, we sought to understand if iNKT cells could shape the distinct biological programs and unique molecular features of TANs. Transcriptomic analysis of sorted CD45⁺Lin⁻CD11b⁺Ly6G⁺ cells from B6 and *Traj18*^{-/-} mice revealed that TANs from B6 animals were enriched for transcripts of chemokines and inflammation-related molecules (*Ccl3*, *Cxcl2*, *Cxcr5*, *Nfkbie*, *Nfkbiz*, *Socs3*, *Atf4*, *Ptsg2*, *Pla2g7*), as well as of immune suppression (*Ii10*, *S100a8*) (Figs. 3F and 3H); these genes have all been associated with different populations of PMN-MDSCs^{24,25}. Additional MDSC markers identified include the C-type lectin domain family 4-member N and D (*Clec4n* and *Clec4d*), activating protein 1 transcription factor subunit (*Junb*) and myeloid cell surface antigen CD33 (*Cd33*)²⁵. Conversely, TANs isolated from *Traj18*^{-/-} showed a marked increased expression of genes associated with MAPK signaling (*Map3k14*, *Map14*,

Fig. 1 iNKT cells infiltrate CRC lesions and correlate with neutrophil abundance. (A) frequency of iNKT cells in adjacent NCT and paired TUM ($n = 115$), with representative dot plots. (B) t-SNE map of iNKT cells based on phenograph metaclustering analysis in NCT and TUM samples. (C) Balloon plot of the scaled integrated MFI of Phenograph clusters generated in B. (D, E) Frequency of IL17⁺GM-CSF⁺ (D) and IFN γ ⁺ (E) iNKT cells infiltrating NCT and TUM; (F) random forest analysis of myeloid and B cell compartment in NCT and TUM with the highest discriminatory power, sorted by mean decrease GINI value. (G) Frequency of neutrophils in NCT and TUM ($n = 75$) with representative plots; (H) Spearman's correlation analysis of IL17⁺GM-CSF⁺iNKT and neutrophils infiltrating NCT and TUM ($n = 25$). $p < 0.05$ (*), $p < 0.01$ (**), $p < 0.001$ ***); Wilcoxon signed-rank test. CD = clusters of differentiation; CRC = colorectal cancer; GM-CSF = granulocyte-monocyte colony-stimulating factor; IFN = interferon; IL = interleukin; iNKT = invariant natural killer T cell; MFI = mean fluorescent intensity; MHC = Major histocompatibility complex; NCT = non-tumor colonic tissue; PD-L1 = programmed death-ligand 1; TNF = tumor necrosis factor; TUM = tumor lesions.



Map12), NETs release (*Hmgb1*, *Hmgb2*, *Ceacam1*, *Mmp15*, *Mmp21*)^{26,27}, the hypoxia inducible factor 1 subunit alpha (*Hif1a*), and the anti-apoptotic BAG cochaperone 4 (*Bag4*) (Figs. 3F and 3H). Pathway enrichment analysis highlighted the upregulation of genes associated with tumor necrosis factor signaling, mostly in B6 TANs (Fig. 3G). To understand if the different transcriptional activity of TANs in B6 and *Trajl18*^{-/-} mice could be restricted to different populations of PMN-MDSCs, we analyzed a publicly available single cell RNA sequencing (sc-RNAseq) dataset of PMN-MDSC from tumor-bearing mice²⁴. The t-distributed stochastic neighbor embedding (t-SNE) overlay analysis revealed the enrichment of the B6 TANs gene signature in a cluster of 'activated' PMN-MDSCs (PMN3), whereas the *Trajl18*^{-/-} TANs gene signature was associated with a population of immature neutrophils/classical PMN-MDSCs (PMN2), reflecting different pathways of PMN-MDSC activation²⁴ in the presence or absence of iNKT cells (Supplementary Fig. 7). Accordingly, we identified two distinct and differentially represented populations of TANs in B6 and iNKT cell-deficient animals. *CD1d*^{-/-} and *Trajl18*^{-/-} mice showed a lower frequency of CD11b⁺Ly6g^{low} TANs and an increase of CD11b⁺Ly6g^{high} TANs (Fig. 3I). CD11b⁺Ly6g^{low} cells had reduced respiratory burst capacity (Fig. 3J), suggesting a diminished cytotoxic potential²⁸, and increased expression of PD-L1 compared with CD11b⁺Ly6g^{high} cells (Fig. 3K). Neutrophil responses to iNKT cells appear to be mediated by both CD1d expression on neutrophils and the iNKT cell activation status because the iNKT cells from tumor-bearing mice induced higher PD-L1 expression in neutrophil from B6 than *CD1d*^{-/-} mice (Supplementary Figs. 8A and 8B). Collectively, these findings reveal that intestinal iNKT cells are associated with different functional subgroups of neutrophils *in vivo*, suggesting a direct iNKT cell-neutrophil crosstalk in CRC pathogenesis.

***In vivo* αGalCer treatment reactivates the cytotoxic potential of iNKT cells**

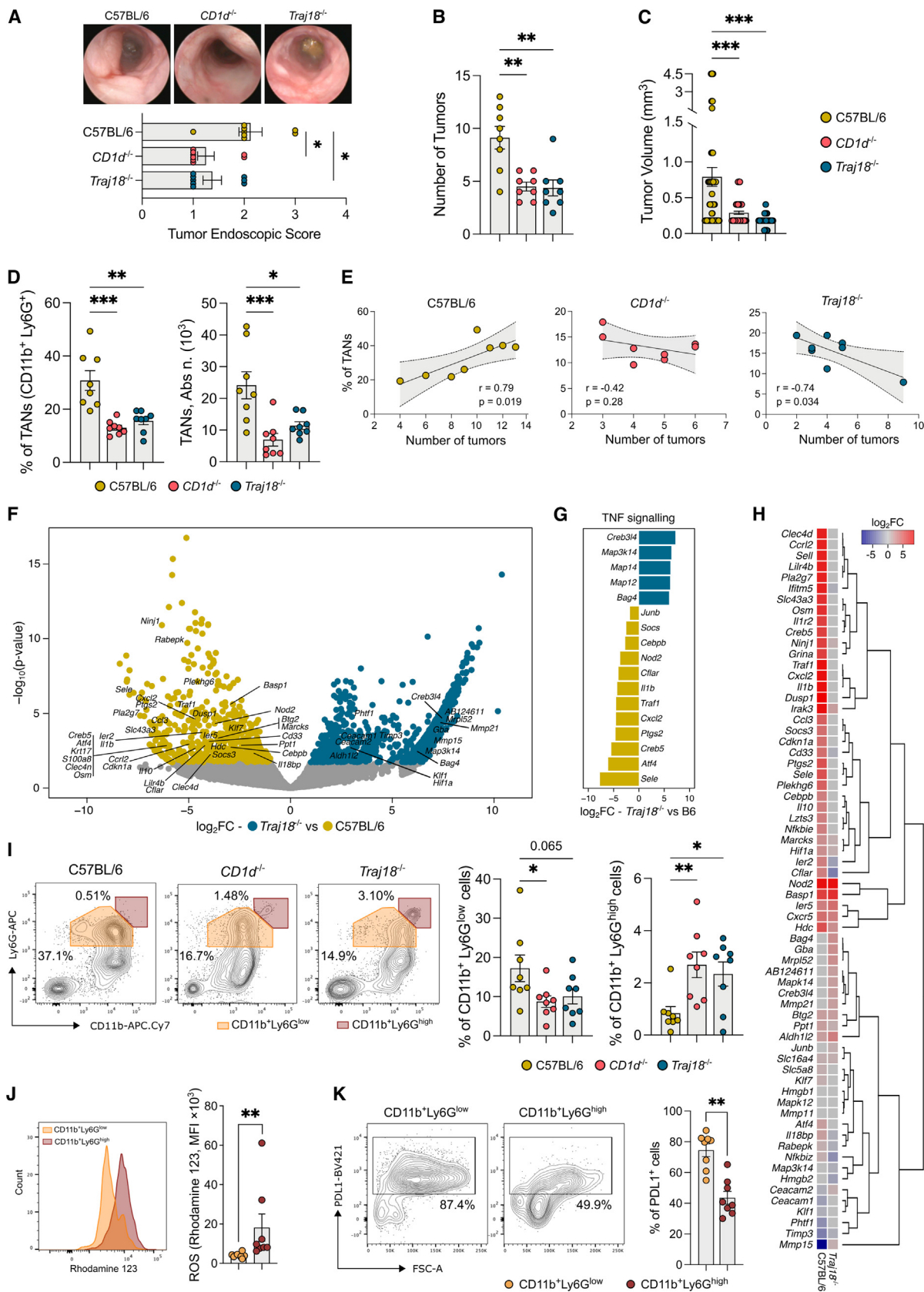
Next, we asked whether we could restore iNKT cells cytotoxicity and induce iNKT-dependent tumor control *in vivo* by using the syngeneic MC38 CRC model. First, we confirmed the pro-tumorigenic role of iNKT cells also in this CRC setting because *Trajl18*^{-/-} mice showed a significantly delayed tumor growth compared with B6 animals (Supplementary Figs. 9A–C) and a reduced infiltration of TANs (Supplementary Fig. 9D). Then, we tested whether the *in vivo* administration of αGalCer to MC38-

bearing B6 mice could restore the anti-tumor phenotype of iNKT cells (Fig. 4A). We found that αGalCer treatment significantly reduced tumor growth (Figs. 4B–D), re-establishing the iNKT cells' ability to express high levels of IFNγ (Fig. 4E). The reconstitution of *Trajl18*^{-/-} mice with splenic iNKT cells promoted tumor growth and TANs infiltration (Fig. 4G–J), whereas αGalCer treatment restored anti-tumor immunity (Fig. 4G–I). Then, we asked whether the intestinal microenvironment could be necessary to skew iNKT cells toward a pro-tumor phenotype (GM-CSF⁺IL17⁺). *In vitro* priming of splenic iNKT cells with the gut microbiota of tumor-bearing AOM-DSS treated mice (B6, *CD1d*^{-/-} and *Trajl18*^{-/-}) induced IL17 and GM-CSF expression in iNKT cells, whereas no effect was observed when iNKT cells were exposed to the gut microbiome of tumor-free mice (Control ROS reactive oxygen species CTRL) (Supplementary Fig. 10). Thus, we performed the orthotopic implantation of MC38 tumor cells into the caecum of B6 animals. We observed that intracaecal MC38 tumors were significantly infiltrated by pro-tumor GM-CSF⁺IL17⁺iNKT cells and TANs (high PD-L1 expression and low ROS production)^{28,29} compared with subcutaneous MC38 tumors (Figs. 4J–L), suggesting that this phenotype is more associated with the presence of an intestinal TME. Finally, αGalCer treatment was still able to promote iNKT cell-mediated anti-tumor immunity in the gut, as measured by longer survival rate, reduced tumor growth, and higher IFNγ expression by iNKT cells in intracaecal tumor-bearing animals (Fig. 4M–Q). These data show that iNKT cells functional phenotype can be manipulated to restore their anti-tumor properties in CRC.

iNKT cell infiltration impairs the favorable prognostic significance of TANs in human CRC and correlates with poor clinical outcomes

Our findings identified a pro-tumorigenic role for iNKT cells in CRC and a functional crosstalk with TANs in murine models. To translate the significance of these results in human CRC, we stratified our patient cohort in tumor-infiltrating iNKT^{high} and iNKT^{low} subgroups and performed Kaplan-Meier analyses. Relapse-free survival at 4 years was higher in iNKT^{low} patients with CRC (Fig. 5A). Several studies described a favorable prognostic significance for neutrophil infiltration in CRC^{30–32}, which we confirmed in our cohort (Fig. 5B); however, the neutrophil positive prognostic significance in CRC was lost with higher infiltration of iNKT cells (Fig. 5C), thus indicating that the beneficial

Fig. 2 *Fusobacterium nucleatum* promotes iNKT cell-mediated recruitment of neutrophils. (A) Bar plot representing the significantly enriched ASVs (FDR $p < 0.05$) in TUM versus NCT mucosal samples ($n = 70$ paired samples from $n = 35$ patients) by DESeq2 analysis. (B) Schematic representation of the experimental plan. (C) Percentage of killing of unstimulated (NS), αGalCer- or *Fn*-primed iNKT cells; results are representative of three ($n = 3$) independent experiments (D) Volcano plot representing the differentially expressed genes in *Fn*- versus αGalCer-primed iNKT cells; the volcano plot shows for each gene (dots) the differential expression (\log_2FC) and its associated statistical significance ($\log_{10}p$ -value). Dots indicate those genes with an FDR-corrected $p < 0.05$ and $\log_2FC > |1.5|$. (E) Gene ontology analysis of the differentially expressed genes (Bonferroni-corrected $p < 0.05$ and $\log_2FC > 1$); (F) Representative histograms (left panels), MFI (middle panels) and frequency (right panels) of IL17⁺, GM-CSF⁺ and IFNγ⁺ iNKT cells unstimulated (NS) or primed with either αGalCer or *Fn*. (G) FC of neutrophils migration index upon exposure to unstimulated (gray bar), αGalCer (blue bars) or *Fn*-primed (red bars) iNKT cell supernatants in the absence (full bars) or presence (pattern fill bars) of Reparixin (20 μM); (H) hIL8 protein concentration in the supernatant released by unstimulated (NS) or αGalCer- or *Fn*-primed iNKT cells; (I) Proliferation index of naïve CD4⁺T cells co-cultured with neutrophils and cell free supernatants from unstimulated (NS), αGalCer, or *Fn* primed iNKT cells. $p < 0.05$ (*), $p < 0.01$ (**), $p < 0.001$ ***); Kruskal-Wallis test. Data are representative of at least three independent experiments. ASV = amplicon sequence variant; CD = clusters of differentiation; CRC = colorectal cancer; ELISA = enzyme-linked immunosorbent assay; FC = fold-change; *Fn* = *F. nucleatum*; FDR = False Discovery Rate; GM-CSF = ; IFN = interferon; IL = interleukin; iNKT = invariant natural killer T cell; MFI = mean fluorescent intensity; NCT = non-tumor colonic tissue; NS = unstimulated; TUM = tumor lesions.



effects of neutrophils on clinical outcomes require the concomitant low infiltration of iNKT cells. Moreover, we validated these results by interrogating the colon adenocarcinoma cohort of The Cancer Genome Atlas database³³ and found that the positive prognosis associated with neutrophil infiltration in patients with CRC (as measured by the expression of the *CEACAM8* gene, encoding for CD66b) was dependent on the low expression of the iNKT cell-specific transcription factor PLZF, encoded by the *ZBTB16* gene³⁴ (Figs. 5D and 5E).

Discussion

iNKT cells are essential components of anti-tumor immune responses due to their massive cytotoxic properties and active participation in immune surveillance against malignant transformation⁹. However, reduced frequencies and functional impairment of iNKT cells associated with the loss of IFN γ secretion³⁵ have been associated with poor overall survival in solid or hematologic tumors⁹. Nevertheless, α GalCer administration can revert iNKT cells functional impairment³⁶, as demonstrated in preclinical studies and clinical trials³⁷. Intriguingly, iNKT cells showed pro-tumor functions also, as reported in the spontaneous murine adenomatous polyposis coli *Apc^{min/+}* model for colon cancer, where iNKT cells promote tumor progression¹⁷.

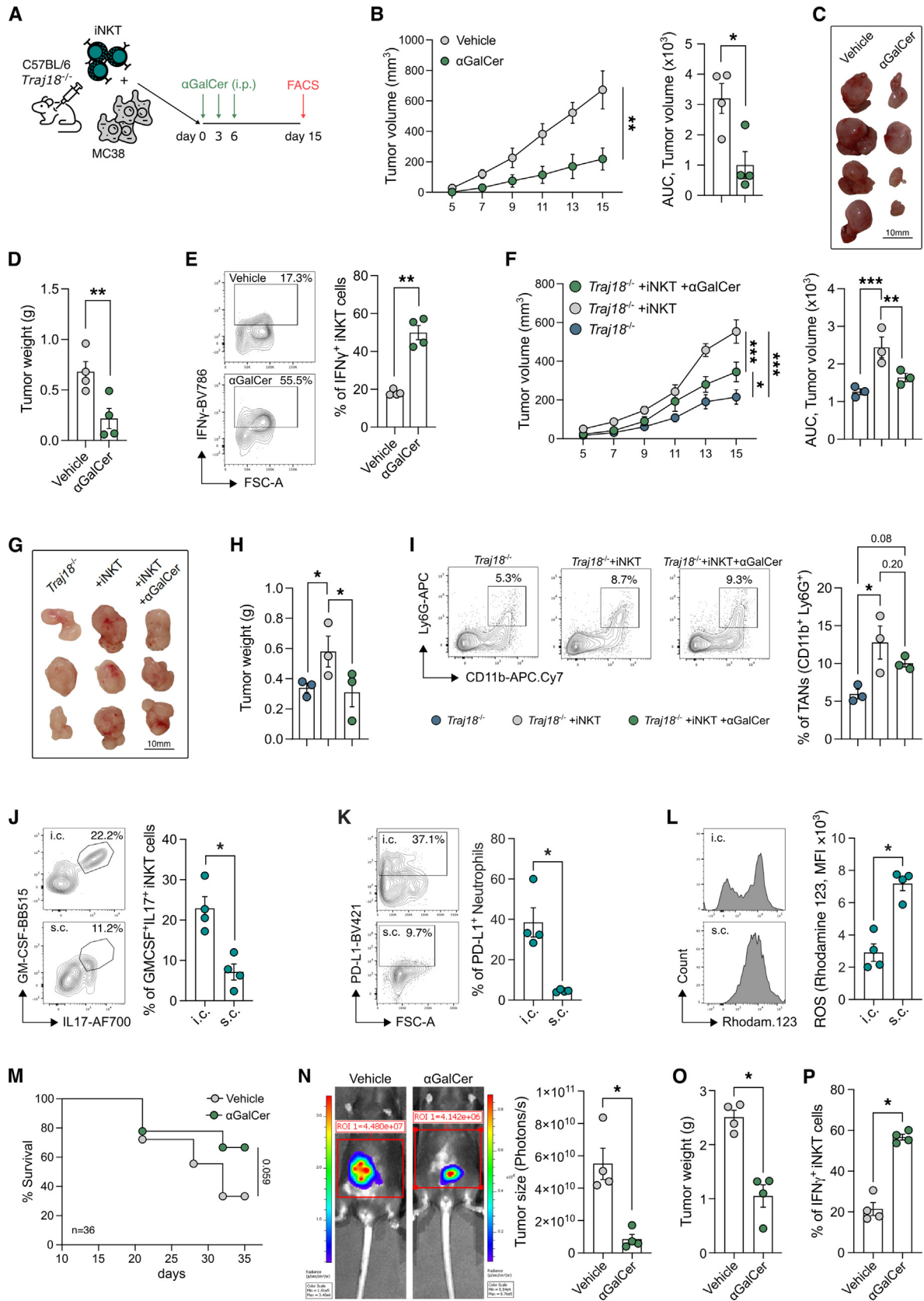
Here, we further expanded these findings by analyzing human CRC specimens and different murine models of CRC, describing the opposing roles of human and murine iNKT cells in paired non-tumor versus cancerous tissue. In this study, the immunophenotypic profiles of *ex vivo* isolated human iNKT cells and the use of two different iNKT cell-deficient murine strains confirmed that IFN γ -producing cytotoxic iNKT cells limit colonic tumorigenesis, whereas the intratumor accumulation of GM-CSF⁺IL17⁺iNKT cells support colon cancer progression.

The gut microbiota is an oncogenic driver of CRC¹⁹ and intestinal microbes represent potent stimulators of iNKT cell responses that can shape their functional plasticity⁶. *Fusobacterium* is a known CRC-associated pathobiont¹⁹ we found enriched in our patient cohort. We show that iNKT cell stimulation with *Fn* promotes their commitment toward a pro-tumor phenotype characterized by the production of IL17 and GM-CSF. *Fn* is known to suppress anti-tumor immunity by binding to the TIGIT receptor on natural killer cells through the virulence factor Fap2³⁸. Accordingly, we observed increased TIGIT expression in tumor-infiltrating iNKT cells. Moreover, *Fn* imprinted a neutrophil chemotaxis gene signature in iNKT cells, with *CXCL8*

being the most upregulated gene. CXCL8, namely IL8, is a chemokine that promotes neutrophil migration which is expressed also by TILs³⁹. By expressing CXCL8, iNKT cells may regulate neutrophils trafficking within the TME, shaping early immune responses in CRC. Our *in vitro* observations and the early tumor infiltration of iNKT cells with respect to neutrophils *in vivo* suggest that this hypothesis may be valid. Few studies report the close interaction of iNKT cells with neutrophils. In melanoma, the active crosstalk of iNKT cells with TANs skews their cytokine production from tolerogenic to pro-inflammatory²¹. In inflammation, neutrophils regulate iNKT cell extravasation in the lung parenchyma²³ and license them to limit the autoimmune responses in the spleen²². In all these studies, the iNKT cell-neutrophil crosstalk relies on CD1d signaling^{21–23}. In our CRC mouse models, iNKT cells modulate the abundance of TANs and affect their phenotype through a CD1d-mediated mechanism. Considering that some chemokines and their receptors, including CXCL8, are absent in mice⁴⁰, we speculate that the recruitment of TANs in our mouse models can be mediated by the expression of other neutrophil chemotaxis genes, such as *CXCL2*, *CXCL3*, and *CCL20*, as suggested by the RNA sequencing (RNA-seq) analysis. We further showed that iNKT cells are necessary to imprint an activated PMN-MDSCs gene signature²⁴ with immune suppressive activity, as demonstrated by the functional assays. The finding that iNKT cells favor neutrophil trafficking within cancer lesions worsening tumor burden is, however, in sharp contrast with previous studies showing that neutrophil infiltration is associated with a better survival in CRC^{30–32}. Nonetheless, the beneficial role of neutrophils in CRC is dependent on iNKT cells because we showed that the concomitant high infiltration of iNKT cells is a negative prognostic factor in our patient cohort and in the colon adenocarcinoma cohort of The Cancer Genome Atlas database. These findings parallel our *in vivo* experiments, where the treatment of tumor-bearing mice with α GalCer reduced tumor burden, suggesting that modulating iNKT cell activation status may be considered a valid therapeutic option to restore their cytotoxic and anti-tumor functions.

Our study shows that tumor-infiltrating iNKT cells can contribute to the remodeling of the TME by recruiting TANs in the early phases of tumor progression, thereby sculpting the CRC developmental trajectory. Our findings uncover the cellular and molecular mechanisms through which the iNKT-TAN axis can suppress anti-tumor immunity in CRC (Fig. 6) and support the targeted manipulation of the function of iNKT cells to

Fig. 3 Absence of iNKT cells reduces tumor formation *in vivo* and infiltration of pro-tumorigenic TANs. (A–C) Cumulative tumor endoscopic score and representative endoscopic pictures (A), number (B) and volume (C) of tumors from AOM-DSS treated C57BL/6, *CD1d*^{-/-} and *Traja18*^{-/-} animals (D) Frequencies (left panels) and absolute numbers (right panels) of TANs in C57BL/6, *CD1d*^{-/-} and *Traja18*^{-/-} animals. (E) Correlation analysis of TANs frequency and number of tumors in C57BL/6, *CD1d*^{-/-}, and *Traja18*^{-/-} animals. (F) Volcano plot representing the DEGs of TANs in C57BL/6 and *Traja18*^{-/-} animals; the volcano plot shows for each gene (dots) the differential expression (log₂FC) and its associated statistical significance (log₁₀*p*-value). Dots indicate those genes with an FDR-corrected *p* < 0.1 and log₂FC > |1|. (G) DEGs enriched in the KEGG TNF signaling pathway (Bonferroni-corrected *p* < 0.05 and log₂FC > |1|). (H) Heatmap and hierarchical clustering of myeloid-derived suppressor cell-related DEGs (FDR-corrected *p*-value < 0.05 and log₂FC > |1|) in neutrophils from C57BL/6 and *Traja18*^{-/-} tumor-bearing versus healthy controls (I) Frequency of CD11b⁺, Ly6G^{high}, and Ly6G^{low} TANs in C57BL/6, *CD1d*^{-/-}, and *Traja18*^{-/-} animals, with representative dot plots. (J, K) Respiratory burst quantification (J) and frequency of PD-L1⁺ (K) in CD11b⁺Ly6G^{high} and CD11b⁺Ly6G^{low} TANs in *Traja18*^{-/-} mice, with representative plots. Data points (*n* = 8) from two pooled independent experiments representative of at least three. *p* < 0.05 (*), *p* < 0.01 (**), *p* < 0.001(***); Kruskal-Wallis and Mann-Whitney tests. Two-tailed Pearson test for correlation analysis. AOM-DSS = azoxymethane-dextran sodium sulfate; CD = clusters of differentiation; DEG = differentially expressed gene; FC = fold-change; FDR = False Discovery Rate; iNKT = invariant natural killer T cell; PD-L1 = programmed death-ligand 1; TNF = tumor necrosis factor; TAN = tumor-associated neutrophils.



improve cancer immunotherapies and adaptive cell transfer therapies based on chimeric antigen receptors/ T cell receptors (CAR/TCR)-engineered iNKT cells⁴¹.

METHODS

Human samples

Tumors and adjacent non-tumor colon tissues were collected with written informed consent from patients (n = 118) diagnosed with CRC between January 2017 and July 2022, who were undergoing surgical resection at Istituto di Ricovero e Cura a Carattere Scientifico (IRCCS) Policlinico Ospedale Maggiore, Milan, Italy, as approved by the institutional review board (Milan, Area B), with permission number 566_2015. American Joint Committee on Cancer (AJCC) IV patients have been excluded from this study. Patient clinical data are summarized in Table 1.

Human cells isolation

Tumor samples were taken transversally to collect both marginal and core tumor zone. Normal adjacent tissues were sampled at least 10 cm from the tumor margin toward the ileum. Human lamina propria mononuclear cells (LPMCs) were isolated as previously described⁴². Briefly, the dissected intestinal mucosa was freed of mucus and epithelial cells in sequential steps with Dithiothreitol (DTT) (0.1 mmol/l) (Microtech, IT) and ethylenediaminetetraacetic acid (EDTA) (1 mmol/l) (Sigma-Aldrich, IT) and then digested with collagenase D (400 U/ml) (Worthington Biochemical Corporation, USA) for 5 hours at 37°C in agitation. LPMCs were then separated with a Percoll gradient.

Neutrophil isolation

Neutrophils were isolated from whole blood samples by dextran sedimentation (4% diluted in Hanks' Balanced Salt Solution HBSS). Red blood cells were lysed using Ammonium-Chloride-Potassium (ACK) lysis buffer (Life Technologies, IT) and neutrophils separated with Percoll (Merck Life Sciences, IT) gradient.

Generation of iNKT cell lines

Human iNKT cell lines were generated from sorted CD45⁺CD3⁺CD1d:PBS57Tet⁺ cells from total LPMCs isolated from intestinal surgical specimens and Peripheral Blood Mononuclear Cells (PBMCs) from healthy donor buffy coats, as previously described⁶. Sorted iNKT cells were stimulated with phytohemagglutinin (1 µg·ml⁻¹, Sigma-Aldrich, IT) and irradiated peripheral blood feeders. PBMCs used as feeders were irradiated at 12.5 Gy. Stimulated cells were then expanded for 15 days by subculturing them every 23 days and maintained in Roswell Park

Memorial Institute (RPMI)-1640 medium with stable glutamine, 5% v/v human serum, and 100 IU·ml⁻¹ IL-2 (Proleukin, Novartis, CH).

Mice

B6(Cg)-Traj18tm1.1Kro/J (*Traj18*^{-/-})⁴³ and B6.129S6-Del(3Cd1d2-Cd1d1)1Sbp/J (*CD1d*^{-/-}) mice⁴⁴ (provided by P. Dellabona, San Raffaele Scientific Institute, Milan, Italy) were previously backcrossed >12 times with C57BL/6 mice. C57BL/6, *Traj18*^{-/-}, and *CD1d*^{-/-} mice were housed and bred at the European Institute of Oncology (IEO) animal facility (Milan, Italy) or at the BIOS+ institute animal facility (Bellinzona, Switzerland) in Specific pathogen Free (SPF) conditions. Sample size was chosen based on previous experience. No sample exclusion criteria were applied. No method of randomization was used during group allocation, and investigators were not blinded. Aged-matched male and female mice were used for experiments. Animal experimentation was approved by the Italian Ministry of Health (Auth. 10/21 and Auth. 1217/20), by the animal welfare committee (Organismo Preposto al Benessere Animale OPBA) of IEO, Italy, and by the Swiss Animal Welfare Office (National n. 34368 and Cantonal n. TI54/2021), Switzerland.

Murine models of carcinogenesis

AOM-DSS model: 7-week-old mice were injected intraperitoneally with 10 mg/kg body weight azoxymethane (AOM, Merck, IT), dissolved in isotonic saline solution. After 7 days, mice were given 1% (w/v) dextran sodium sulfate (DSS MW 40 kD; TdB Consultancy, Sweden) in their drinking water for 7 days, followed by 14 days of recovery. The cycles were repeated 2 or 3 times and mice sacrificed at day 49 or 70.

Subcutaneous MC38 model

The 7-week-old mice were injected subcutaneously with 4×10^5 MC38 cells. Tumor volume (V) was calculated from the caliper measurements using the following formula: $V = (W^2 \times L)/2$, where W is the tumor width and L is the tumor length⁴⁵. A total of 2 µg of αGalCer was injected intraperitoneally on days 0, 3, and 6. iNKT reconstitution in *Traj18*^{-/-} mice was performed co-inoculating freshly sorted splenic iNKT with MC38 cells at 1:4 ratio. Tumor-bearing animals were sacrificed after 15 days or earlier when showing any sign of discomfort.

Intracaeal MC38 model

The 7-week-old mice were intracaeally injected with 4×10^5 MC38 cells in a 1:1 solution of PBS and Matrigel (Corning), as pre-

Fig 4 *In vivo* αGalCer administration restores iNKT cell anti-tumor functions. (A) Schematic representation of experimental plan. (B-D) MC38 tumor growth with their relative AUC (B), representative pictures (C) and weight of tumors (D) from MC38-bearing C57BL/6 mice treated with vehicle or αGalCer. (E) Frequency of tumor-infiltrating IFNγ⁺iNKT cells in MC38-bearing C57BL/6 animals treated with vehicle or αGalCer, and representative dot plots. (F-I), MC38 tumor growth and AUC (F), representative pictures (G), weight of tumors (H) and frequency of TANs (I) in MC38-bearing *Traj18*^{-/-} animals reconstituted, or not, with iNKT cells prior to treatment with αGalCer. (J) Frequency of GM-CSF⁺IL17⁺iNKT cells in i.c. and s.c. MC38-bearing mice. (K) Frequency of PD-L1⁺ and (L) respiratory burst quantification in CD11b⁺Ly6G⁺ TANs from i.c. and s.c. MC38-bearing mice. (M) Frequency of survival of intracaeal MC38-bearing mice treated with vehicle or αGalCer (n = 18 per group). (N) Tumor burden calculated by Photons/s with IVIS representative pictures and (O) tumor weights from intracaeal MC38-bearing mice treated with vehicle or αGalCer. (P) Frequency of tumor-infiltrating IFNγ⁺iNKT cells in intracaeal MC38-bearing mice treated with vehicle or αGalCer. Data shown (n = 3-4 per group) are representative of at least one of two independent experiments. p < 0.05 (*), p < 0.01 (**), p < 0.001(***). Mann-Whitney, Kruskal-Wallis tests and two-way analysis of variance for tumor growth. ; AUC = Area Under the Curve; CD = clusters of differentiation; GM-CSF = granulocyte-monocyte colony-stimulating factor; i.c. = intracaeal; IFN = interferon; iNKT = invariant natural killer T cell; MFI = mean fluorescent intensity; PD-L1 = programmed death-ligand 1; s.c. = subcutaneous; TAN = tumor-associated neutrophils.

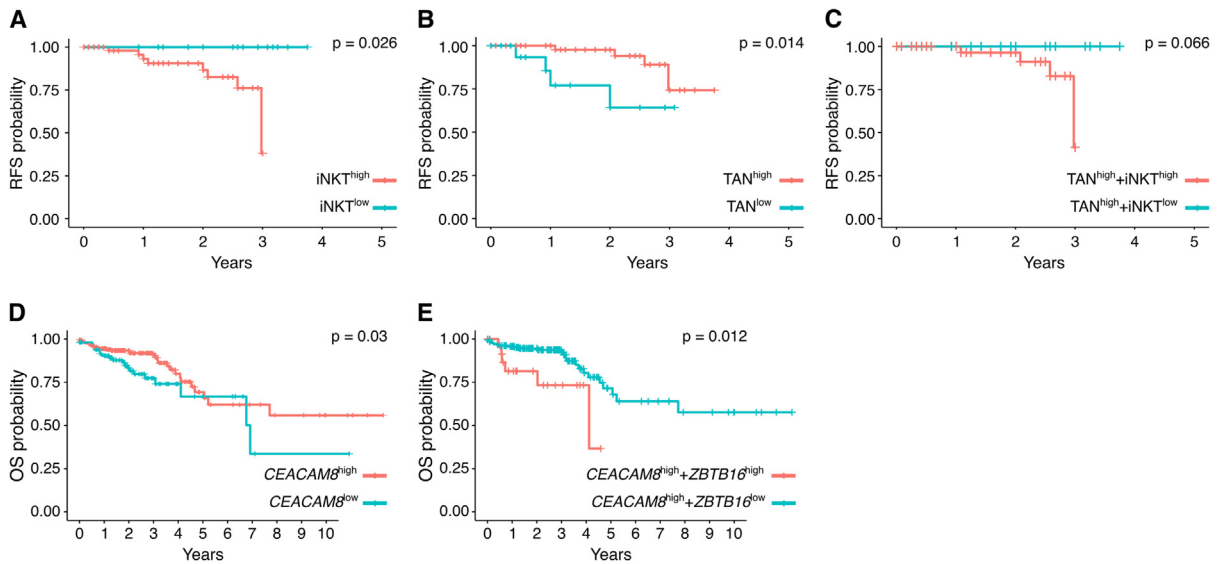


Fig. 5 iNKT cell infiltration correlates with poor patient outcomes. (A–C) Kaplan-Meier RFS curves of patients with CRC from Policlinico Hospital, Milan presenting high versus low (A) tumor-infiltrating iNKT cells, (B) high versus low TANs or (C) high versus low tumor-infiltrating iNKT cells in the population of TAN^{high} patients. (D–E) Kaplan-Meier OS curves of patients with CRC from The Cancer Genome Atlas cohort with respect to (D) high or low expression of *CEACAM8* within tumor specimens and (E) high or low expression of *ZBTB16* in the in the population of *CEACAM8*^{high} patients. CRC = colorectal cancer; iNKT = invariant natural killer T cell; OS = overall survival; RFS = relapse-free survival; TAN = tumor-associated neutrophils.

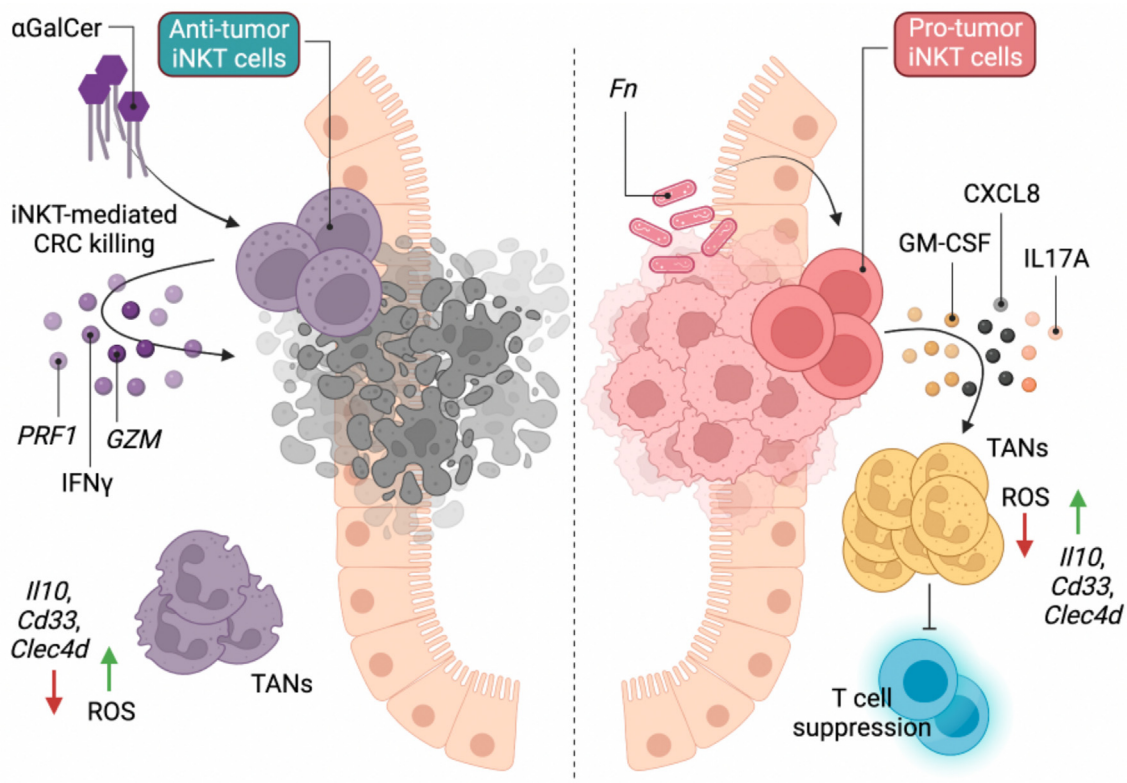


Fig. 6 Proposed model for iNKT cell-mediated pro/anti-tumor immunity in CRC. The CRC-associated pathobiont *Fn* impairs iNKT cell cytotoxic functions and promotes a pro-inflammatory phenotype in iNKT cells. Moreover, iNKT cell conditioning by *Fn* promotes iNKT cell-mediated recruitment of neutrophils with phenotypic and functional characteristics ascribable to polymorphonuclear myeloid-derived suppressor cells in the tumor microenvironment (panel on the right of the dotted line). Our findings indicate that restoring the cytotoxic potential of iNKT cells by treating them with α GalCer leads to control of tumor growth (panel on the left of the dotted line). CD = clusters of differentiation; CRC = colorectal cancer; GM-CSF = granulocyte-monocyte colony-stimulating factor; IFN = interferon; IL = interleukin; iNKT = invariant natural killer T cell; *Fn* = *F. nucleatum*; PRF = perforin; ROS = reactive oxygen species; TAN = tumor-associated neutrophils.

viously described⁴⁶. Mice were checked every day for the first week and starting from day 7, they were weighed once a week. Tumor growth was measured on the IVIS Spectrum (Caliper LifeSciences, USA) upon administration of D-luciferin (GoldBio, USA). For α GalCer treatment mice were injected intraperitoneally with 2 μ g of α GalCer on days 7, 10, and 13. Tumor-bearing animals were sacrificed after 35 days or earlier when showing any sign of discomfort.

Murine colonoscopy

Colonoscopy was performed weekly for tumor monitoring using the Coloview system (TP100 Karl Storz, Germany). Tumor endoscopic score has been quantified as previously described⁴⁷. During the endoscopic procedure, mice were anesthetized with 3% isoflurane.

Murine cells isolation

Single-cell suspensions were prepared from the colon of C57BL/6, *Trajp18*^{-/-}, and *CD1d*^{-/-} mice, as previously described⁸. Briefly, cells were isolated through incubation with 5 mM EDTA at 37°C for 30 minutes, followed by mechanical disruption with GentleMACS (Miltenyi Biotec, Germany). After filtration with 100- μ m and 70- μ m nylon strainers (BD), the LPMC were counted and stained for immunophenotyping. MC38 tumors were digested with collagenase D (0.75 mg/ml, Merck, IT) and Dnase I (0.1 mg/ml, Merck, IT) in RPMI-1640+2% Fetal bovine serum (FBS) at 37°C for 60 minutes. Cell suspension was filtered through 70- μ m cell strainers, washed, counted, and stained for multiparametric flow cytometry.

Fn culture condition

Fn strain ATCC25586 was maintained on Columbia agar supplemented with 5% sheep blood or in Columbia broth (Difco, Detroit, MI, USA) under anaerobic conditions at 37°C. Columbia broth was supplemented with hemin at 5 μ g·ml⁻¹ and menadione at 1 μ g·ml⁻¹. Bacterial cell density was adjusted to 1 \times 10⁷ colony forming unit (CFU)·ml⁻¹ and heat-killed at 95°C for 15 minutes before being stored at -80°C until use in downstream experimentation.

α GalCer and *Fn*-priming of iNKT cell

moDCs were pulsed with α GalCer (100 ng/ml) or with heat-inactivated *Fn* (4 \times 10⁵ CFU) and co-cultured with iNKT cells (2 \times 10⁵ cells) in a 2:1:4 iNKT:moDC:*Fn* ratio in RPMI-1640 supplemented with 10% FBS, Pen/Strep. After 24 hours, iNKT cell activation status was estimated by intracellular staining.

iNKT cell cytotoxicity assay

iNKT cell cytotoxicity toward the human CRC cell lines Colo205 and RKO (American Type Culture Collection) was performed as previously described¹⁵.

iNKT-neutrophil co-culture assay

α GalCer or *Fn*-primed iNKT cells (2 \times 10⁵ cells) were co-cultured with freshly isolated neutrophils in a 1:1 ratio in RPMI-1640 supplemented with 10% FBS. After 24 hours, the cells were stained for extracellular markers expression and ROS detection.

In vitro suppression assay

N \ddot{a} ive CD4⁺T cells were isolated from PBMCs of healthy donors (CD4-n \ddot{a} ive human microbeads, Miltenyi Biotec). Cells were labeled with 1 nM Far Red CellTrace (ThermoFisher, IT), resus-

ended in medium containing hIL2 (Proleukin, Novartis, CH) and anti-CD28 antibody (2 μ g/ml, Tonbo, USA), and plated in 96-well plates (NUNC Maxisorp) pre-coated with anti-CD3 antibody (2 μ g/ml, Tonbo) at a concentration of 2.5 \times 10⁴ cells/well. Freshly isolated neutrophils were co-cultured with T cells at a 1:1 ratio and the culture supernatant from NS, α GalCer, or *Fn*-primed iNKT cells were added at a final concentration of 10%. After 5 days, proliferating n \ddot{a} ive CD4⁺T cells were labeled with Zombie vital dye (Biolegend, IT) and analyzed with a BD FACS Celesta. The suppression index was calculated using the FlowJo proliferation modeling tool and normalized on minimum proliferation levels.

Neutrophil migration assay

Freshly isolated neutrophils were first pre-incubated 20 minutes at 37°C with reparixin (20 μ M) or RPMI-1640+2%FBS and then seeded on top of a 3 mm-pore transwell (SARSTEDT, IT) in 200 μ l of RPMI-1640+2%FBS. A total of 500 μ l of chemoattracting medium, i.e. the culture supernatant of activated iNKT cell lines diluted 10% in RPMI-1640+2% FBS (see the α GalCer and *Fn*-priming of iNKT cell protocol), was added on the bottom of the transwell and neutrophil migration was allowed for 4 hours at 37°C. RPMI-1640+10% FBS was used as positive control. After 4 hours of incubation, the total number of cells on the bottom of the plate were stained and counted using the FACSCelesta flow cytometer (BD Biosciences, Franklin Lakes, NJ, USA) with plate-acquisition mode and defined volumes.

Neutrophil survival assay

Freshly isolated neutrophils were cultured with RPMI-1640+10% FBS supplemented with the culture supernatants (10%) from α GalCer or *Fn*-primed iNKT cells for 16 hours at 37°C. Cells were then stained with FITC Annexin V Apoptosis Detection Kit with 7-AAD (Biolegend, IT) following the manufacturer's instruction and acquired at a FACS Celesta flow cytometer (BD Biosciences, Franklin Lakes, NJ, USA).

Respiratory burst assay

ROS production was quantified using the neutrophil/monocyte respiratory burst assay (Cayman, USA) following the manufacturer's instructions.

Enzyme-linked immunosorbent assay

Detection of IL8/CXCL8 in culture supernatants was performed using the OptEIA Human IL-8 kit (BD Biosciences, IT), according to the manufacturer's instruction.

Gut microbiota-priming of murine iNKT cells

Splenic iNKT cells were isolated from C57BL/6 mice sorting CD45⁺CD3⁺CD1d:PB557Tet⁺ cells upon enrichment through B cells exclusion (Mouse CD19 microbeads, Miltenyi Biotec, Germany). Bone marrow-derived dendritic cells from C57BL/6 mice were pulsed with heat-inactivated fecal microbiota of controls or AOM-DSS treated C57BL/6, *Trajp18*^{-/-}, and *CD1d*^{-/-} mice and co-cultured with freshly isolated splenic iNKT cells (2 \times 10⁵ cells) in a 2:1:10 iNKT:bone marrow-derived dendritic cells:microbiota ratio in RPMI-1640 supplemented with 10% FBS and Pen/Strep solution. After 24 hours, the iNKT cell activation status was estimated by intracellular staining. Fecal samples were resuspended 1:10 (w/v) in PBS and filtered through a 0.75- μ m filter to remove large debris; microbiota cell density was quantified by quantitative Polymerase Chain Reaction (qPCR)⁴⁸, adjusted to 2 \times 10⁷

CFU·mL⁻¹, and heat-killed at 95°C for 15 minutes before being stored at -80°C until use in downstream experimentation.

Co-culture of iNKT cells with bone marrow-derived cells

Liver iNKT cells were isolated from AOM-DSS tumor-bearing and control C57BL/6 mice sorting for CD45⁺CD3⁺CD1d:PBS57Tet⁺ cells. iNKT cells were co-cultured with bone marrow-derived cells from either C57BL/6 or *CD1d*^{-/-} animals in a 1:1 ratio for 24 hours in RPMI-1640 supplemented with 10% FBS.

Flow cytometry

Cells were washed and stained with the combination of mAbs purchased from different vendors, as listed in [Supplementary Table 2](#). iNKT cells were stained and identified using human or mouse CD1d:PBS57 Tetramer (National Institutes of Health Tetramer core facility) diluted in PBS with 1% heat-inactivated FBS for 30 minutes at 4°C. For intracellular cytokine labeling, cells were incubated for 3 hours at 37°C in RPMI-1640+10% FBS with phorbol myristate acetate (PMA) (50 ng/ml, Merck, IT), ionomycin (1 µg/ml, Merck), and brefeldin A (10 µg/ml, Merck, IT). Before intracellular staining, cells were fixed and permeabilized using Cytofix/Cytoperm (BD). Samples were analyzed with a FACSCelesta flow cytometer (BD Biosciences, Franklin Lakes, NJ, USA) or a BD FACSymphony™ A5 (BD Biosciences, Franklin Lakes, NJ, USA). Data were analyzed using the FlowJo software (Version 10.8, TreeStar, Ashland, OR, USA). For the multidimensional analysis using t-SNE visualization and phenograph clustering⁴⁹, refer to the dedicated section in the [supplementary material](#). Briefly, FCS files were quality checked for live singlets and antibody agglomerates and normalized to avoid batch effects. Multidimensional regression and clustering analysis were performed using the cytofkit package through the cytofkit graphical user interface (GUI).

Bulk RNA sequencing of human iNKT cells

Total RNA (from 1 × 10⁶ cells) was isolated with the RNeasy kit (Qiagen, IT) and RNA quality was checked with the Agilent 2100 Bioanalyzer (Agilent Technologies, IT). A total of 0.5–1 µg were used to prepare libraries for RNA-seq with the Illumina TruSeq RNA Library Prep Kit v2 following the manufacturer's instructions. RNA-seq libraries were then run on the Agilent 2100 Bioanalyzer (Agilent Technologies, IT) for quantification and quality control and pair-end sequenced on the Illumina NovaSeq platform.

Bulk RNA-seq of sorted neutrophils

Total RNA from ~ 5 × 10⁵ neutrophils (CD45⁺Lin⁻CD11b⁺Ly6G⁺) was isolated with the RNeasy micro kit (Qiagen, IT) and RNA quality was checked with the Agilent 2100 Bioanalyzer (Agilent Technologies, IT). Sequencing libraries were prepared by using the NEBNext rRNA Depletion Kit v2 and the NEBNext Ultra II Directional RNA Library Prep kits following the manufacturer's instructions. RNA-seq libraries were then run on the Agilent 2100 Bioanalyzer (Agilent Technologies, IT) for quantification and quality control and pair-end sequenced on the Illumina NovaSeq platform.

RNA-seq data analysis

RNA-seq reads were preprocessed using the FASTX-Toolkit tools. Quality control was performed using FastQC. Pipelines for the primary analysis (filtering and alignment to the reference genome of the raw reads) and secondary analysis (expression quan-

tification, differential gene expression) have been integrated and run in the HTS-flow system⁵⁰. Differentially expressed genes were identified using the Bioconductor Deseq2 package⁵¹. P-values were false discovery rate corrected using the Benjamini-Hochberg procedure implemented in DESeq2. The functional enrichment analyses to determine gene ontology categories and KEGG pathways were performed using the DAVID Bioinformatics Resources (DAVID Knowledgebase v2022q2) (<https://david.ncifcrf.gov>)⁵².

Statistical analysis

Statistical tests were conducted using Prism (Version 8.2.0, GraphPad, USA) software or the R software (version 3.6.2). Paired non-parametric Wilcoxon test was used to compare non-tumor and tumor tissues, both in human and murine samples. The Mann-Whitney U test was used for unpaired comparisons. Spearman's correlation coefficient was used for the analysis of correlations. Random forest⁵³ analysis of flow cytometric data from innate immune cells was performed using the randomForest R package; permutation tests with 1000 permutations were performed to assess model significance. Kaplan-Meier analysis were carried out using the R packages *survival* (version 3-2-11) and *survminer* (version 0.4.9). Statistical analyses were always performed as two-tailed. The *p*-values were corrected for multiple comparisons and considered statistically significant with *p* < 0.05. ****p* < 0.001; ***p* < 0.01; **p* < 0.05.

AUTHOR CONTRIBUTIONS

FF conceived the study. FF, GL, and FS designed the experiments. GL, FS, ADB, FP, CA, LI, AB, and MRG performed the experiments. FF and FS supervised the experiments. FC, MV, FG, GI, and LM contributed with reagents and resources. FC, DN, MV, MG, LB, EC, and BG recruited patients. GL performed multidimensional FACS data analysis. FS performed RNA sequencing (RNA-seq) and metagenomics data analyses. GP performed scRNA-seq analysis. LP and ET performed FACS cells sorting. FN helped with the design of RNA-seq experiments. FF, FS, and GL wrote the manuscript. All authors reviewed and critically edited the manuscript. The co-first authorship order was determined by considering the early career stage. Both GL and FS contributed equally and have the right to list their name first in their CV. All authors contributed to the article and approved the submitted version.

DECLARATIONS OF COMPETING INTEREST

The authors have no competing interests to declare.

FUNDING

This work was made possible thanks to the financial support of Associazione Italiana per la Ricerca sul Cancro (Start-Up 2013 14378, Investigator Grant - IG 2019 22923 to FF) and of Italy's Ministry of Health (GR-2016-0236174 to FF and FC). This work has been and partially supported by the Italian Ministry of Health with Ricerca Corrente and 5X1000 fund.

DATA AVAILABILITY

RNA sequencing data are available in the ArrayExpress database (<http://www.ebi.ac.uk/arrayexpress>) under accession numbers E-MTAB-12278 and E-MTAB-12281. 16S rRNA gene sequencing data are available in the European Nucleotide Archive (<https://www.ebi.ac.uk/ena>) under accession number PRJEB56178. The PMN-MDSC scRNA-seq dataset is publicly avail-

able at GEO (<https://www.ncbi.nlm.nih.gov/geo/>) under accession number GSE163834.

ACKNOWLEDGMENTS

The authors thank the IEO Animal Facility for the excellent animal husbandry, the IEO Genomic Unit for the support in high throughput sequencing, and the National Institutes of Health Tetramer Facility for providing human and murine CD1d:PBS57 tetramers. The authors are grateful to the équipe of the General and Emergency Surgery Unit, Ospedale Maggiore Policlinico, Milano for their tireless work. The authors thank Dr. Paolo Dellabona and Dr. Giulia Casorati for providing *CD1d*^{-/-} and *Traj18*^{-/-} mice. The authors thank Prof Maria Rescigno, Prof Massimo C. Fantini, Dr Matteo Marzi, and Dr Roberto Gianbruno for the helpful discussions and support in the setup of sequencing experiments. The authors thank Claudia Burrello and Erika Mileti for initial setups of the experiments. Schemes in Figs. 2B and 4A were created using icons from the Noun Project (<https://the-nounproject.com/>). Fig. 6 was created with BioRender.com (<https://biorender.com/>). The authors thank the Associazione Italiana per la Ricerca sul Cancro and the European Association for Cancer Research for the financial support to GL.

APPENDIX A. SUPPLEMENTARY DATA

Supplementary data to this article can be found online at <https://doi.org/10.1016/j.mucimm.2023.03.006>.

REFERENCES

- Crosby, C. M. & Kronenberg, M. Tissue-specific functions of invariant natural killer T cells. *Nat. Rev. Immunol.* **18**, 559–574 (2018).
- Brigl, M. & Brenner, M. B. How invariant natural killer T cells respond to infection by recognizing microbial or endogenous lipid antigens. *Semin. Immunol.* **22**, 79–86 (2010).
- Facciotti, F. et al. Peroxisome-derived lipids are self antigens that stimulate invariant natural killer T cells in the thymus. *Nat. Immunol.* **13**, 474–480 (2012).
- Díaz-Basabe, A., Strati, F. & Facciotti, F. License to kill: when iNKT cells are granted the use of lethal cytotoxicity. *Int. J. Mol. Sci.* **21**, 3909 (2020).
- Constantinides, M. G. & Belkaid, Y. Early-life imprinting of unconventional T cells and tissue homeostasis. *Science* **374**, eabf0095 (2021).
- Burrello, C. et al. Mucosa-associated microbiota drives pathogenic functions in IBD-derived intestinal iNKT cells. *Life Sci. Alliance* **2**, e201800229 (2019).
- Burrello, C. et al. Therapeutic faecal microbiota transplantation controls intestinal inflammation through IL10 secretion by immune cells. *Nat. Commun.* **9**, 5184 (2018).
- Burrello, C. et al. IL10 secretion endows intestinal human iNKT cells with regulatory functions towards pathogenic T lymphocytes. *J. Crohns Colitis* **16**, 1461–1474 (2022).
- Delfanti, G., Dellabona, P., Casorati, G. & Fedeli, M. Adoptive immunotherapy with engineered iNKT cells to target cancer cells and the suppressive microenvironment. *Front. Med. (Lausanne)* **9**:897750.
- Deo, S. V. S., Sharma, J. & Kumar, S. GLOBOCAN 2020 Report on global cancer burden: challenges and opportunities for surgical oncologists. *Ann. Surg. Oncol.* **29**, 6497–6500 (2022).
- Chen, J., Pitmon, E. & Wang, K. Microbiome, inflammation and colorectal cancer. *Semin. Immunol.* **32**, 43–53 (2017).
- Fan, X. & Rudensky, A. Y. Hallmarks of tissue-resident lymphocytes. *Cell* **164**, 1198–1211 (2016).
- Tachibana, T. et al. Increased intratumor Valpha24-positive natural killer T cells: a prognostic factor for primary colorectal carcinomas. *Clin. Cancer Res.* **11**, 7322–7327 (2005).
- Metelitsa, L. S. et al. Natural killer T cells infiltrate neuroblastomas expressing the chemokine CCL2. *J. Exp. Med.* **199**, 1213–1221 (2004).
- Díaz-Basabe, A. et al. Human intestinal and circulating invariant natural killer T cells are cytotoxic against colorectal cancer cells via the perforin-granzyme pathway. *Mol. Oncol.* **15**, 3385–3403 (2021).
- Krijgsman, D. et al. Characterization of circulating T-, NK-, and NKT cell subsets in patients with colorectal cancer: the peripheral blood immune cell profile. *Cancer Immunol. Immunother.* **68**, 1011–1024 (2019).
- Wang, Y. et al. Unique invariant natural killer T cells promote intestinal polyps by suppressing TH1 immunity and promoting regulatory T cells. *Mucosal Immunol.* **11**, 131–143 (2018).
- Cortesi, F., Delfanti, G., Casorati, G. & Dellabona, P. The pathophysiological relevance of the iNKT cell/mononuclear phagocyte crosstalk in tissues. *Front. Immunol.* **9**, 2375 (2018).
- Garrett, W. S. The gut microbiota and colon cancer. *Science* **364**, 1133–1135 (2019).
- Brossay, L. et al. CD1d-mediated recognition of an alpha-galactosylceramide by natural killer T cells is highly conserved through mammalian evolution. *J. Exp. Med.* **188**, 1521–1528 (1998).
- De Santo, C. et al. Invariant NKT cells modulate the suppressive activity of IL-10-secreting neutrophils differentiated with serum amyloid A. *Nat. Immunol.* **11**, 1039–1046 (2010).
- Häggglöf, T. et al. Neutrophils license iNKT cells to regulate self-reactive mouse B cell responses. *Nat. Immunol.* **17**, 1407–1414 (2016).
- Thanabalasuriar, A., Neupane, A. S., Wang, J., Krummel, M. F. & Kubers, P. iNKT cell emigration out of the lung vasculature requires neutrophils and monocyte-derived dendritic cells in inflammation. *Cell Rep.* **16**, 3260–3272 (2016).
- Veglia, F. et al. Analysis of classical neutrophils and polymorphonuclear myeloid-derived suppressor cells in cancer patients and tumor-bearing mice. *J. Exp. Med.* **218**, e20201803 (2021).
- Alshetaiwi, H. et al. Defining the emergence of myeloid-derived suppressor cells in breast cancer using single-cell transcriptomics. *Sci. Immunol.* **5**, eaay6017 (2020).
- Rayes, R. F. et al. Neutrophil extracellular trap-associated CEACAM1 as a putative therapeutic target to prevent metastatic progression of colon carcinoma. *J. Immunol.* **204**, 2285–2294 (2020).
- Shaul, M. E. & Fridlender, Z. G. The dual role of neutrophils in cancer. *Semin. Immunol.* **57**:101582.
- Gershkovitz, M. et al. TRPM2 mediates neutrophil killing of disseminated tumor cells. *Cancer Res.* **78**, 2680–2690 (2018).
- He, G. et al. Peritumoural neutrophils negatively regulate adaptive immunity via the PD-L1/PD-1 signalling pathway in hepatocellular carcinoma. *J. Exp. Clin. Cancer Res.* **34**, 141 (2015).
- Wikberg, M. L. et al. Neutrophil infiltration is a favorable prognostic factor in early stages of colon cancer. *Hum. Pathol.* **68**, 193–202 (2017).
- Tosti, N. et al. Infiltration by IL22-producing T cells promotes neutrophil recruitment and predicts favorable clinical outcome in human colorectal cancer. *Cancer Immunol. Res.* **8**, 1452–1462 (2020).
- Ponzetta, A. et al. Neutrophils driving unconventional T cells mediate resistance against murine sarcomas and selected human tumors. *Cell* **178**, 346–360.e24 (2019).
- Network, C. G. A. R. et al. The Cancer Genome Atlas Pan-Cancer analysis project. *Nat. Genet.* **45**, 1113–1120 (2013).
- Kovalovsky, D. et al. The BTB-zinc finger transcriptional regulator PLZF controls the development of invariant natural killer T cell effector functions. *Nat. Immunol.* **9**, 1055–1064 (2008).
- Tahir, S. M. et al. Loss of IFN-gamma production by invariant NK T cells in advanced cancer. *J. Immunol.* **167**, 4046–4050 (2001).
- Terabe, M. & Berzofsky, J. A. The immunoregulatory role of type I and type II NKT cells in cancer and other diseases. *Cancer Immunol. Immunother.* **63**, 199–213 (2014).
- Zhang, Y. et al. α-GalCer and iNKT Cell-Based Cancer Immunotherapy: realizing the Therapeutic Potentials. *Front. Immunol.* **10**, 1126 (2019).
- Gur, C. et al. Binding of the Fap2 protein of *Fusobacterium nucleatum* to human inhibitory receptor TIGIT protects tumors from immune cell attack. *Immunity* **42**, 344–355 (2015).
- Crespo, J. et al. Human naive T cells express functional CXCL8 and promote tumorigenesis. *J. Immunol.* **201**, 814–820 (2018).
- Eruslanov, E. B., Singhal, S. & Albelda, S. M. Mouse versus human neutrophils in Cancer: a major knowledge gap. *Trends Cancer* **3**, 149–160 (2017).
- Delfanti, G. et al. TCR-engineered iNKT cells induce robust antitumor response by dual targeting cancer and suppressive myeloid cells. *Sci. Immunol.* **7**, eabn6563 (2022).
- Caprioli, F. et al. Autocrine regulation of IL-21 production in human T lymphocytes. *J. Immunol.* **180**, 1800–1807 (2008).
- Cui, J. et al. Requirement for Valpha14 NKT cells in IL-12-mediated rejection of tumors. *Science* **278**, 1623–1626 (1997).
- Smiley, S. T., Kaplan, M. H. & Grusby, M. J. Immunoglobulin E production in the absence of interleukin-4-secreting CD1-dependent cells. *Science* **275**, 977–979 (1997).
- Bousquet, P. F. et al. Preclinical evaluation of LU 79553: a novel bis-naphthalimide with potent antitumor activity. *Cancer Res.* **55**, 1176–1180 (1995).

46. Cremonesi, E. et al. Gut microbiota modulate T cell trafficking into human colorectal cancer. *Gut* **67**, 1984–1994 (2018).
47. Becker, C., Fantini, M. C. & Neurath, M. F. High resolution colonoscopy in live mice. *Nat. Protoc.* **1**, 2900–2904 (2006).
48. Furet, J. P. et al. Comparative assessment of human and farm animal faecal microbiota using real-time quantitative PCR. *FEMS Microbiol. Ecol.* **68**, 351–362 (2009).
49. Brummelman, J. et al. Development, application and computational analysis of high-dimensional fluorescent antibody panels for single-cell flow cytometry. *Nat. Protoc.* **14**, 1946–1969 (2019).
50. Bianchi, V. et al. Integrated systems for NGS data management and analysis: open issues and available solutions. *Front. Genet.* **7**, 75 (2016).
51. Love, M. I., Huber, W. & Anders, S. Moderated estimation of fold change and dispersion for RNA-seq data with DESeq2. *Genome Biol.* **15**, 550 (2014).
52. Sherman, B. T. et al. David: a web server for functional enrichment analysis and functional annotation of gene lists (2021 update). *Nucleic Acids Res.* **50**, W216–W221 (2022).
53. Breiman, L. Random forests. *Mach. Learn.* **45**, 5–32 (2001).